Original Article

Impact of Acquisition Protocols on Accuracy of Dose Calculation Based on XVI Cone Beam Computed Tomography

Slimani Souleyman[1,2], Khalal Dorea Maria[3], Tyeb Cheikh[1], Khalal-Kouache Karima[2]

[1]Department of Radiotherapy, HCA Hospital, Kouba, [2]SNIRM Laboratory, Faculty of Physics, University of Sciences and Technology Houari Boumediene, Algiers, ALGERIA, [3]Dosage, Analyse and Characterisation in High Resolution Laboratory, Department of Physics, Ferhat Abbas Setif 1 University, Setif, Algeria

Abstract

Purpose: The objective of this work is to study the impact of acquisition protocols on the accuracy of cone beam computed tomography (CBCT)-based dose calculation and to determinate its limits from image characteristics such as image quality, Hounsfield numbers consistency, and restrictive sizes of volume acquisition, compared to the CT imaging for the different anatomy localizations: head and neck (H&N), thorax, and pelvis. **Materials and Methods:** In this work, we used a routine on-board imaging CBCT of the XVI system (Elekta, Stockholm, Sweden). Dosimetric calculations performed on CT images require the knowledge of the Hounsfield unit-relative electron density (HU-ReD) calibration curve, which is determined for each imaging technology and must be adapted to the imaging acquisition parameters (filter/field of view). The accuracy of the dose calculation from CBCT images strongly depends on the quality of these images and also on the appropriate correspondence to the electronic densities, which will be used by the treatment planning system to simulate the dose distribution. In this study, we evaluated the accuracy of the dose calculation for each protocol, as already pointed in many studies. **Results:** As a result, the protocols that give better results in terms of dose calculation are F0S20 for the H&N region and F1M20 for the thoracic and pelvic regions, with an error <2% compared to results obtained with CT images. In addition, the dose distributions obtained with CT and CBCT imaging modalities were compared by two different methods. The first comparison was done by gamma index in three planes (sagittal, coronal, and transverse) with 2%; 2 mm criteria. The results showed good correspondence, with more than 95% of points passed the criteria. We also compared the target volume, the organs at risk (OARs), and the maximum and minimum doses for the three localizations (H&N, thorax, and pelvis) in CT and CBCT imaging modalities using a Rando phantom. **Conclusions:** The choice of the adequate CBCT acquisition protocol and the appropriate phantom to determine the HU-ReD calibration curve provides a better precision in the calculation of dose on CBCT images. This allows improving the results obtained when using the HU-ReD calibration method for dose calculation in adaptive radiotherapy.

Keywords: Adaptive radiotherapy, calibration curve, cone beam computed tomography, Hounsfield units

Received on: 29-12-2020 **Review completed on: 19-04-2021** **Accepted on: 23-04-2021** **Published on: 07-08-2021**

Introduction

In external radiotherapy, the dose is calculated from the patient's anatomical information acquired during the virtual simulation (computed tomography [CT]), which is performed a few days before starting the patient's treatment. Thus, the realization of the treatment plan is based on the anatomy of a fixed day. However, radiotherapy treatment consists of several daily irradiation sessions lasting several weeks, and positional and anatomical variations can occur during treatment causing a discrepancy between the distribution of the dose delivered to the patient and that planned.[1,2]

The main objective of adaptive radiotherapy (ART) is to take into account and correct these variations. Its development has become possible by embedded imaging on linear accelerators.[3,4] Cone beam CT (CBCT) volume images of the patient can thus be acquired in the treatment room, offering the possibility of a new delineation of volumes and a new calculation of the dose distribution.

Kilo-voltage (kV)-CBCT was implemented to verify the patient's positioning on the treatment table before the

Access this article online

Quick Response Code:

Website: www.jmp.org.in

DOI: 10.4103/jmp.JMP_128_20

Address for correspondence: Dr. Slimani Souleyman, Department of Radiotherapy, HCA Hospital, Kouba, Algiers, Algeria. SNIRM Laboratory, Faculty of Physics, University of Sciences and Technology Houari Boumediene, Algiers, Algeria. E-mail: soly_slimani@yahoo.fr

How to cite this article: Souleyman S, Maria KD, Cheikh T, Karima KK. Impact of acquisition protocols on accuracy of dose calculation based on XVI cone beam computed tomography. J Med Phys 2021;46:94-104.

irradiation session. This system has proven its importance, especially for techniques of treatment with intensity modulation such as intensity-modulated radiotherapy (IMRT) or volume-modulated arc therapy (VMAT). However, its use for dosimetric purposes remains an interesting concept. Indeed, kV-CBCT would allow a rapid and accurate assessment of the dose distribution,[5-8] despite its limitation in image characteristics such as image quality, Hounsfield numbers consistency, and restrictive sizes of acquisition volume comparing to the CT.

The calculation of the dose from CBCT images requires the knowledge of attenuation coefficients, expressed in Hounsfield units (HU) contained in the voxels of the image. The conversion of these HUs to relative electron densities (ReDs) is required for the dose calculation using the treatment planning system (TPS).[9] The Hounsfield numbers in CBCT images depend on many parameters, unlike in CT images because of the conical geometry of the beam of CBCT and therefore of a more pronounced scattering than for a CT acquisition.

In the literature, we can find different strategies for CBCT-based dose calculation as the establishment of Hounsfield numbers versus ReD curves,[9-13] the density override to regions of interest (ROIs), the deformable registration between CT and CBCT images, and the deep learning method to generate pseudo-CT.[9,14-19] Literature results show that discrepancies between the reference CT-based dose calculation and the CBCT-based dose calculation are often lower than 3%, regardless of the method. However, they can also reach 10% with unsuitable method. Even if the accuracy of the CBCT-based dose calculation is dependent of the method, some strategies are promising but need improvements in the automating process for routine implementation.[9]

In this article, we present a study of the impact of acquisition protocols on the accuracy of CBCT-based dose calculation with HU-ReD calibration curve method, and we determine its limits from image characteristics for the different anatomy localizations: head and neck (H&N), thorax, and pelvis. Our goal is to improve the precision given by this method compared to other ones well described in the literature.[18,19] These methods that have proven their efficiency in terms of precision are more complex than the method studied in this paper. The improvement of the quality of this method is carried out by choice of the adequate acquisition parameters to have a better quality of CBCT image and by the selection of the calibration phantom, which gives less error in the HU-ReD calibration curve.

Materials and Methods

Image acquisition

For the acquisition of the CT images, we used the simulator scanner (Big Bore, Philips). These CT images were considered as a reference to which the CBCT images were compared. The detection system of the CT scanner has 51 modules and each module contains 16 detectors. Acquisition parameters are reported in Table 1 for three anatomical locations: H&N, thorax, and pelvis.

CBCT images were acquired with an X-ray volume Imager (XVI®, Elekta System) mounted on the gantry of an Elekta Synergy® linear accelerator (Elekta, Stockholm, Sweden). It is composed of an X-ray tube and a planar detector made of amorphous silicon/cesium iodide, which is placed perpendicularly to the treatment axis. The XVI® system uses a conical beam to acquire the entire volume during a single rotation of the accelerator. All acquired projections are used to reconstruct the volume images of conic tomography. The irradiation parameters corresponding to the XVI® acquisition protocols proposed by the manufacturer and that are used in the context of this study are reported in Table 2.

Volumetric images can be acquired using three different fields of view (FOVs) depending on the acquisition protocol used: small (S), medium (M), and large (L). The size of the FOV corresponds to a lateral displacement of the center of the detector in the direction perpendicular to the axis of the kV energy beam (0 mm, 115 mm, and 190 mm for fields of view S, M, and L, respectively). For each FOV, there are three additional collimators (marked 10, 15, and 20) in the form of cassettes inserted at the outlet of the X-ray tube to vary the length of the imaged volume. In the same way, two cassettes corresponding to the presence (F1) or not (F0) of a butterfly filter can be inserted at the exit of the X-ray tube.[10]

In this study, we have considered the protocols F0S10 and F0S20 for the H&N region, F0M20 and F1M20 for the thoracic region, and F0M20, F1M20, and F1L20 for the pelvic region.

Phantoms

To establish HU-ReD calibration curves, two different phantoms available in our department were used: the Catphan®503 phantom[20] and the Gammex® Phantom (TomoTherapy "Cheese," RMI, Model 467).[21] The Catphan®503 phantom contains a specific heterogeneous module (CTP 404) with seven different inserts. The "Cheese" phantom is usually

Table 1: Irradiation parameters related to the computed tomography simulator acquisition protocols

	H&N	Thorax	Pelvis
Tube voltage (kVp)	120	120	140
mAs/slice	325	250	300
Collimation (mm)	16×0.75	16×0.75	16×0.75
Slice thickness (mm)	2	3	3

H&N: Head and neck

Table 2: Irradiation parameters related to XVI® acquisition protocols

	F0S10	F0S20	F1M20	F0M20	F1L20
Tube voltage (kVp)	100	100	120	120	120
Total mAs	36.1	39.3	1038.4	144.7	1661.4
Rotation (°)	100	180	360	360	360

used for quality assurance of helical tomotherapy machines. This phantom is an 18 cm thick solid water cylinder with a diameter of 30 cm. It consists of two semicylindrical halves, in which a film can be placed. There are 20 plugs, including four solid water plugs plus 16 tissue substitute plugs that range in electron density relative to water from 0.28 to 1.69. These plugs can be inserted into 28 mm diameter holes in the "Cheese" phantom. The inserted plugs as shown in Figure 1 are representative of the range of inhomogeneities observed in the clinical environment.[5]

An anthropomorphic Rando Anderson phantom was used to study the impact of the different protocols considered in this study on the accuracy of dose calculation based on CBCT images. It is of adult human form and consists of a human skeleton embedded in tissue-equivalent material. It is divided into 35 separate slices with a thickness of 2.5 cm. Each slice has a raster of 3 cm × 3 cm with holes for the insertion of thermoluminescent dosimeters (TLDs) [Figure 1]. The location of organs and tissue in the slices were determined with the aid of an atlas of CT anatomy[22] and drawings of the phantom slices.

Hounsfield unit-relative electron density calibration curves determination

To determine HU-ReD calibration curves for both the CT and CBCT, we measured the mean HU values with a ROI of 8 mm^2 circle for all inserted materials from the different phantoms [Figure 2]. They were then plotted as a function of the corresponding ReD [given by phantom manufacturers in Table 3]. HU-ReD-CBCT established curves on each phantom (i.e., HU-ReD-CBCT-GMX for Gammex and HU-ReD-CBCT-CTP for Catphan) were determined for all acquisition protocols. To carry out this study well, we investigated each FOV (S, M, and L) separately as well as its specifications in terms of collimation and filtering as given by the manufacturer. This would show the impact of the phantom and the acquisition parameters choice for the determination of the calibration curves on the accuracy of dose calculation. However, the standard deviations in the ROIs for each insert in the CBCT images were higher compared to those for the CT images. This fact also shows the difference in image quality and Hounsfield numbers given by CT and CBCT images. This can be explained by the scatter and the reduction of CBCT projection number compared to the CT.

The reference curve was the HU-ReD-CT curve implemented into the TPS for clinical plans. This curve was used for HU-ReD conversion before dose calculation for all CT images.

Dose calculation using cone beam computed tomographic images

The HU-ReD calibration curves depend on the acquisition parameters (FOV, tube voltage, mAs, etc.) which change from one protocol to another. These curves are dependent also on the region in the patient to be imaged which directly affects the CBCT image quality acquired by the system.

We studied the choice of acquisition protocol for the XVI Elekta system suitable for the three anatomical locations (H&N, thorax, and pelvis) and which would give more precision for the dose calculation on CBCT images in different ballistic scenarios in three-dimensional conformal radiotherapy (3D CRT), VMAT, and IMRT for step and shoot (S&S) and sliding window (SW).

To evaluate the accuracy of the dose calculation on CBCT image acquisitions, we simulated ballistics of the real treatment for the different localizations (H&N, thorax, and pelvis) by taking examples of the most frequent cases in each region (brain tumor, pulmonary neoplasia, and prostate tumor) [Figure 3].

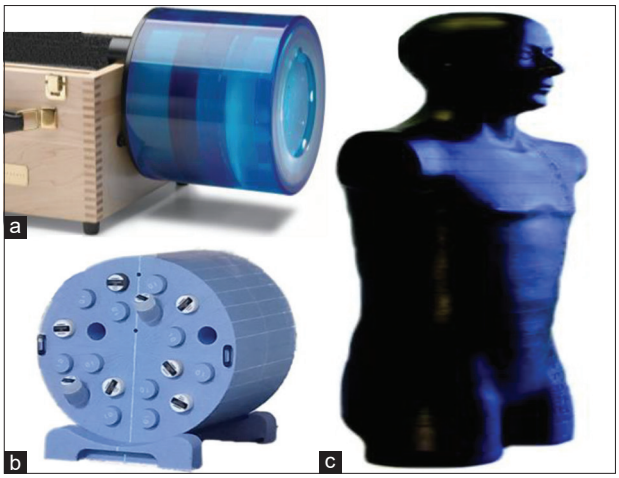

Figure 1: Phantoms used in this study: (a) Catphan, (b) Gammex, and (c) Rando Anderson

Table 3: Materials of Gammex and Catphan plugs

Gammex plugs		Catphan plugs	
Material	**ReD**	**Material**	**ReD**
Air	0	Air	0
Lung (LN300)	0.28	PMP	0.853
Lung (LN450)	0.43	LDPE	0.945
Water	1	Polystyrene	0.998
Inner Bone (IB3)	1.09	Water	1
Calcium (CB2-30%)	1.26	Acrylic	1.147
Calcium (CB2-50%)	1.45	Delrin	1.363
Cortical bone (SB3)	1.69	Teflon	1.868

ReD: Relative electron density

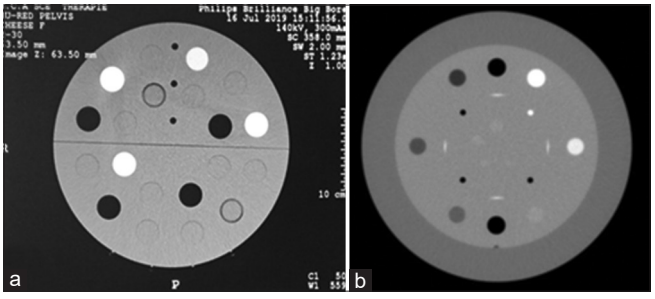

Figure 2: The axial slice of the phantoms (a) Gammex and (b) Catphan

To avoid any other source of error that may arise, we started this evaluation step on a Rando Anderson phantom, which has the morphology of a real patient by showing the impact of the image quality in CBCT acquisitions for the protocols chosen in the previous section on the accuracy of the dose calculation. In this manner, we eliminate two factors that can influence the results when using a real patient and which are morphological changes and movement artifacts.

The interest volumes and treatment plans were simulated on the CT images and then exported to the CBCT images by a rigid registration of CT-CBCT images. All the structures and irradiation parameters were thus identical on the two series of images CT and CBCT.

To study the protocol impact on the accuracy of the dose calculation, the calibration curves for each protocol were used to calculate the dose with heterogeneity corresponding to the treatment plans by delivering 200 cGy for the following cases:

- Anterior field
- Two right and left side fields
- Four orthogonal fields (box technique)
- IMRT plan (S&S and SW)
- VMAT plan.

The dose is calculated for different protocols applied in different anatomical regions of the Rando phantom. After that, the dose distributions of the two CT and CBCT imaging modalities are compared using Verisoft software (v 6.0, PTW Freiburg, Germany)[23] and the gamma index method for three comparison planes (sagittal, coronal, and transverse) with 2%; 2 mm criteria. We also compare the coverage of the target volume and the OARs, as well as the maximum and minimum doses for the three diseases and for the two CT and CBCT imaging modalities.

Results

Hounsfield unit-relative electron density calibration curves

The calibration curves obtained for the CT acquisitions with the two phantoms and for the different localizations are presented in Figure 4a. The curves denoted CTP and GMX correspond, respectively, to the Catphan and Gammex phantoms. First, we notice that the calibration curves are practically identical for both H&N and thorax protocols. However, for the pelvis protocol, we note a very slight difference in high densities region (Teflon) when we used the Catphan phantom. A maximum difference of 43 HU which corresponds to 4.6% is observed. However, the largest difference (131 HU) corresponding to the acquisitions using the Gammex phantom is observed in the densest insert (Cortical Bone SB3). This value represents a relative difference of 10.7% for the pelvis protocol (CT-PELVIS-GMX).

Furthermore, a large difference is observed between the calibration curves obtained with the Catphan phantom and those obtained with the Gammex phantom within isodense ROIs. The difference is more evident for higher densities than that of water [Figure 4a]. The largest difference between HU-ReD-CT-GMX and HU-ReD-CT-CTP is observed for a CT number of 1200 HU corresponding to a variation of the relative density Δ ReD = 0.41 for the thorax protocol.

Unlike what was observed in the case of CT imaging, the difference between the calibration curves given by Catphan and those given by Gammex for CBCT imaging [Figure 4b-d] is not observed only for the high values of the relative electronic densities but also for the low ones. These curves are similar in the ReD range equivalent to water. By comparing the calibration curves for CT and CBCT, we notice that there is a shift between these curves of 727 ± 159 HU for the protocol S and 576 ± 141 HU for the protocols M and L. The largest difference between planning CT and CBCT was observed for the air-insert. The CT value in the planning CT was nearly zero, while the pixels in the CBCT were ranging from 535 to 1370 HU depending of the protocol type. For the F1M20 and F1L20 protocols, the difference in CT values was reduced for denser materials such as Delrin® and Teflon® for Catphan phantom and Cortical Bone SB3 for Gammex phantom. However, the difference was more evident for the low electronic densities for the F0S20 and F0S10 protocols.

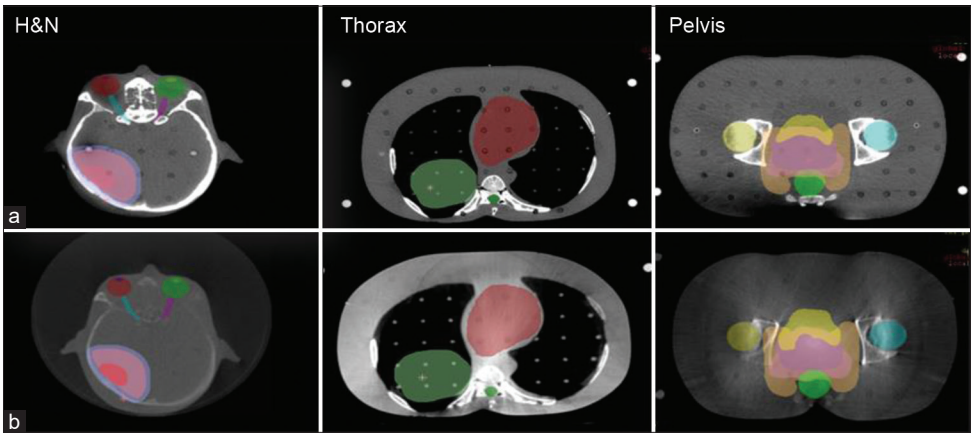

Figure 3: (a) Computed tomography and (b) cone beam computed tomography images of the Rando Anderson phantom for the different anatomy localizations (H&N, thorax and pelvis). H&N: Head and neck

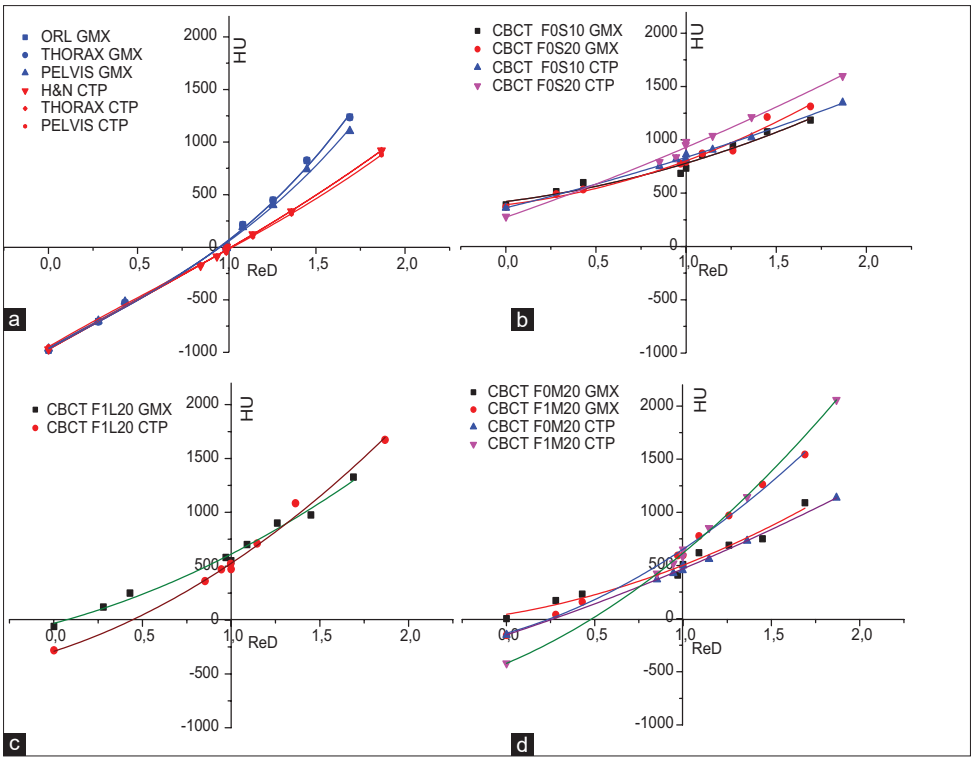

Figure 4: (a) HU-ReD-CT calibration curves with Gammex phantom (GMX, blue) and Catphan phantom (CTP, red). **(b)** HU-ReD-CBCT calibration curves with Gammex and Catphan phantoms for the protocol S. (c) HU-ReD-CBCT calibration curves with Gammex and Catphan phantoms for the protocol L. (d) HU-ReD-CBCT calibration curves with Gammex and Catphan phantoms for the protocol M. HU-ReD: Hounsfield unit-relative electron density, CT: Computed tomography, CBCT: Cone beam computed tomography

The dose calculation based on CT or CBCT images strongly depends not only on the image quality but also on the precision of the ReD values given by the HU-ReD calibration curves. Figure 5a and b shows for the same values of HU, the ReD given by each HU-ReD calibration curve determined for the different acquisition protocols and by the two phantoms used in this study [Catphan in Figure 5a and Gammex in Figure 5b]. The greatest difference was observed for the values lower than 500 HU which can have ReD values varying between 0 (air) for all CBCT acquisitions and 0.47 ± 0.02 in CT acquisitions. For a value of 1000 HU, the ReD varies for CBCT between 0.31 and 0.99 depending on the protocol and especially the presence or not of the filter F, whereas for CT, the ReD varies between 1.28 and 1.53 which depends much more on the phantom used (Catphan or Gammex).

Impact of the cone beam computed tomography image acquisition protocol on the dose calculation

The relative differences in the calculated dose using the different acquisition protocols in CBCT compared to the reference which is the dose calculated from CT acquisitions are evaluated and presented in Figure 6. Each relative difference is evaluated by calculating the dose error at the isocenter for each treatment plan.

These results show that the relative error in the dose calculation in CBCT increases with the complexity of the treatment plan (number of fields). There is less than 1% error for a single field whereas this value increases toward more than 2% even 4.25% for the F0M20 protocol for the use of a VMAT plan with two arcs.

In the H&N region, the F0S20 protocol gives better results and less error compared to F0S10. These errors do not exceed 2%, except in one case (with 2.19%) corresponding to the IMRT SW plan with 7 fields. However, in the thoracic region, the protocol with a filter F1M20 gives satisfactory results compared to the acquisition protocol without filter F0M20 for which the errors range between 0.74% for a single field up to 3.17% for a plan with two arcs. The errors of the dose calculation with F1M20 do not exceed 2.11% for the VMAT plan with two arcs and 0% for a single field compared to the dose calculated on the CT acquisitions. However, in the pelvic region, we compared three protocols F0M20, F1M20, and F1L20 in the dose calculation in CBCT. The obtained results confirm that the use of the filter improves the precision of dose calculation, especially in this region where the difference is clearer than in the thoracic region. The dose calculation errors obtained using the F1L20 protocol are also satisfactory: Less than 0.35% for plans with direct fields, less than 1.67% for IMRT plans, and less than 2.16% for VMAT plans. However, the maximal error observed by the use of F1M20 in the pelvic region is 1.89% for the plan in IMRT SW with 7 fields.

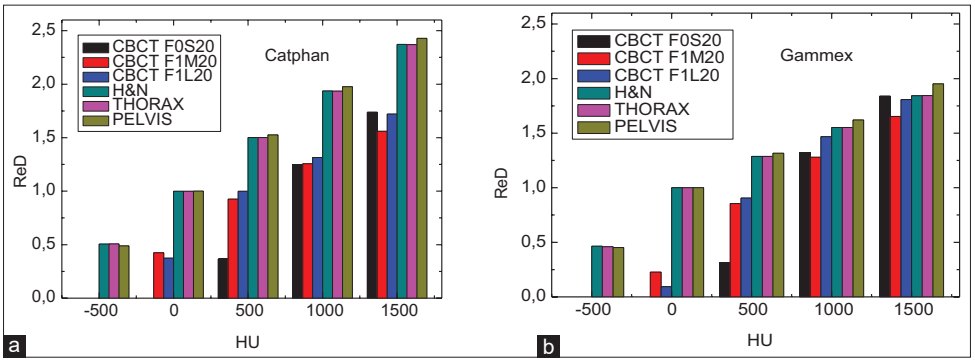

Figure 5: Variation of the relative electronic density according to the corresponding Hounsfield units values for different CT and CBCT acquisition protocols with the Catphan phantom (a) and the Gammex phantom (b). CT: Computed tomography, CBCT: Cone beam computed tomography

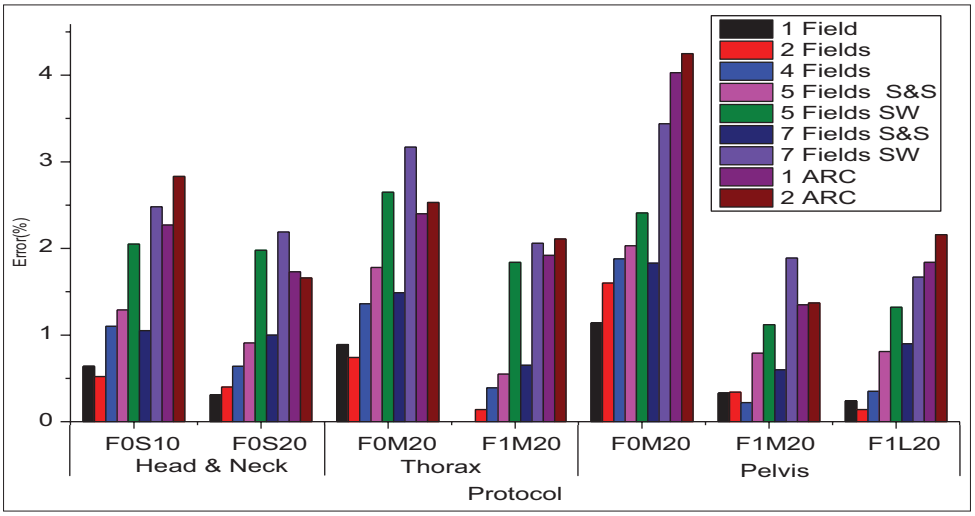

Figure 6: Relative difference of the calculated dose in CBCT according to the CBCT acquisition protocols used compared to those obtained with CT images. CT: Computed tomography, CBCT: Cone beam computed tomography, S&S: Step and shoot, SW: Sliding window

According to these results, one can conclude that the protocols which give better results in terms of dose calculation when compared with dose calculation using CT calibration curves are F0S20 in the H&N region and F1M20 in the thoracic and pelvic regions.

Dose calculation using cone beam computed tomography images

To evaluate the dose distribution on the CBCT images in the Rando Anderson phantom, we used the H&N, thorax, and pelvis parts of this phantom. The advantage of using this anthropomorphous phantom lies in the absence of problems of repositioning over time. In addition, with this phantom, we have no problem related to taking into account a tumor and/or a weight loss as for a real patient.

We performed CT and CBCT acquisitions of the Rando Anderson phantom by reproducing the same position on the table using the simulator scanner and the accelerator positioning lasers. We have made CT treatment plans with 3D CRT for three different pathologies: brain tumor (glioblastoma), lung neoplasia, and prostatic tumor. These plans were made on the CT images by using the calibration curves given by the Catphan phantom and those given by the Gammex phantom. They were directly exported to the CBCT images to ensure the position match between the isocenters used, respectively, for the CT and CBCT dose calculation. Thus, all the structures and irradiation parameters are identical on the two sets of CT and CBCT images. The goal is to compare the dose distributions on both imaging modalities.

To compare the different dose distributions given by the calibration curves determined previously, we calculated the percentages of the differences in the dose constraints by taking the dose distribution given by the HU-ReD-CT-CTP calibration curve as a reference. In Figures 7-9, we show the difference in coverage of planning target volumes (PTVs) by the calculation of D2%, D50%, D98% and DMax for each PTV and for H&N, lung neoplasia, and pelvis cases, respectively. On the other hand we also show the impact of this dose distribution on the OARs.

Head and neck case

The results of planning for a H&N pathology on the Rando phantom using the calibration curves given by the Catphan

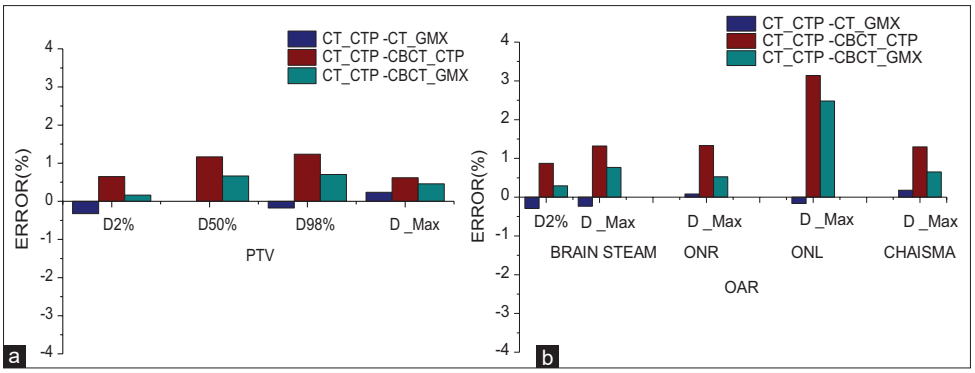

Figure 7: The percentage of dose differences in the dosimetric parameters of the PTV (a) and OARs (brainstem, optic nerves, and chiasm) (b) in plans calculated using different calibration curves of CT and CBCT. CT: Computed tomography, CBCT: Cone beam computed tomography, PTV: Planning target volume, OAR: Organ at risk

phantom and those given by the Gammex phantom for the two imaging modalities CT and CBCT (with the protocol F0S20) are presented in Figure 7. The percentages of dose differences in the dosimetric parameters of the PTV [Figure 7a] and OARs (brainstem, optic nerves, and chiasm) [Figure 7b] in plans are calculated using different calibration curves of CT and CBCT.

In the coverage of the target volumes, the difference noted in the same CT imaging modality but using the HU-ReD-CT-CTP and HU-ReD-CT-GMX calibration curves does not exceed 0.3%. While using the CBCT acquisitions the difference in the dose distribution in the PTV is more remarkable ,which show an increase in maximum dose of 0.61%, D50% of 1.16% and the maximum difference is 1.23% in D98% which is noted for the distribution given by HU-ReD-CBCT-CTP [Figure 7a].

However, the difference between CT and CBCT for OARs remains below 1.48 Gy which corresponds to 3.14% for the left optic nerve and 1.32% for the brainstem using the UH-ReD-CT-CTP calibration curve. The difference was less than 2.48% for the right optic nerve and 0.77% for the brainstem using the UH-ReD-CT-GMX calibration curve [Figure 7b]. Despite this reduction in doses for CBCT imaging, the dose constraints are still respected for PTV and also for OARs.

Thorax case

In this case of lung pathology, the acquisition of the CBCT images was realized with the protocol F1M20. The planning of the treatment on the Rando phantom used the calibration curves obtained with the phantoms Catphan and Gammex. The obtained results are shown in Figure 8.

The dose coverage results of the target volumes show more similarity between the dose distributions calculated by the CT images using the curves established with the two phantoms (the difference is 0.27% in DMax and 0.32% in D98%) [Figure 8a]. This shows in the case of thoracic pathology, that the use of one of the phantoms (Catphan or Gammex) for the determination of the calibration curve for the CT will not have a significant influence on the obtained dose distribution.

However, the results on the CBCT acquisitions show a greater difference compared to the results on CT given by HU-ReD-CT-CTP calibration curve: 0.94% in DMax and 1.13% in D98% for the use of HU-ReD-CBCT-CTP. This difference considerably increased when we used the calibration curve determined by Gammex phantom HU-ReD-CBCT-GMX: 3.6% in absolute value for Dmax and 3.71% for D98% for the coverage of PTVs. However, the results of the OARs given in Figure 8b show that the use of the HU-ReD-CBCT-GMX calibration curve can give more differences which exceed the accepted tolerances such as 5.88% in D2% in spinal cord and 4.7% in DMean in heart. On the other hand, the distribution given by the use of the HU-ReD-CBCT-CTP curve gives better results on OARs with a difference that does not exceed 3.7% in D2% in the heart.

Pelvis case

We acquired CT and CBCT images of the pelvis portion of the Rando Anderson phantom with the acquisition parameters defined in Table 1 for the CT and the F1M20 protocol [Table 2] for the CBCT. In this case, we show again that the use of the two phantoms (Catphan and Gammex) to determine the CT calibration curves used in the planning of treatment on the TPS does not have a significant difference. Indeed, the use of HU-ReD-CT-CTP or HU-ReD-CT-GMX give percentages in dose differences lower than 1% for the coverage of PTVs and for the dose constraints of OARs for the pelvic region.

However, the results of the dose calculations on the CBCT acquisitions show decreases in the coverage of PTVs up to − 1.17%. The differences in the dose distribution in OARs do not exceed 1.34%. This is obtained when using the HU-ReD-CBCT-CTP calibration curve. The results are less good when using HU-ReD-CBCT-GMX for dose calculation on CBCT acquisitions. The results shown in Figure 9 give maximum differences of 1.78% in DMax and 1.85% in D98% for PTV46, while on OARs, we have 1.94% in D30% for the bladder and 1.57% in D50% for the rectum, as the maximum of the differences.

These results also show that in this case of the pelvic region, the dose calculation on CBCT acquisitions with the F1M20

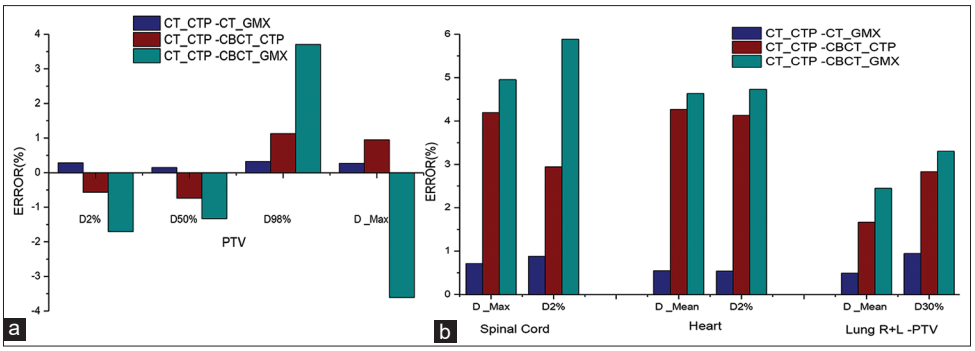

Figure 8: The percentages of dose differences in the dosimetric parameters of the PTV (a) and OARs (spinal card,heart and lung) (b) in plans calculated using different calibration curves of CT and CBCT

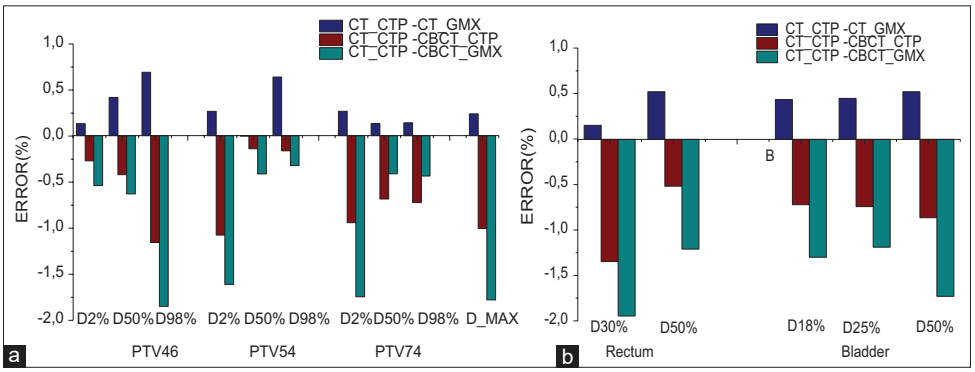

Figure 9: The percentages of dose differences in the dosimetric parameters of the PTVs (a) and OARs (b) in plans calculated using different calibration curves of CT and CBCT. CT: Computed tomography, CBCT: Cone beam computed tomography, PTV: Planning target volume, OAR: Organ at risk

protocol gives satisfactory results with differences which do not exceed 2% for the two calibration curves used in this study determined by the Catphan and Gammex phantoms.

Comparison of dose distributions

The results obtained from the gamma index for the various planes are shown in Table 4. They show a good correspondence between the CT [Figure 10a] and CBCT [Figure 10b] dose distributions with a slight difference in the extremities and especially in the regions of low dose which are well shown in Figure 10c. This figure represents the regions corresponding to the difference between the two distributions to be compared and which does not satisfy the comparison criteria 2%, 2 mm.

Table 4 summarizes the percentage of points that pass the 2%, 2 mm criterion in the planes where this comparison was made (sagittal, frontal, and transverse planes) for each location studied previously. We note that we obtain more than 95% of points which pass the criterion. The thoracic region corresponds to the lowest percentage compared to the other regions. Thus, we confirm the previous results of comparison on coverage of the target volumes and the satisfaction of the dose constraints of the OARs as described in the previous sections.

Table 4: Results of the gamma index (%) for the different dose distribution plans of the head and neck, thorax, and pelvis parts

	H&N	Thorax	Pelvis
Sagittal	96.4	95.9	98.4
Frontal	95.9	95.8	96.9
Transverse	98.6	97.5	99.3

H&N: Head and neck

Discussion

Our results in this study show that the calibration HU-ReD-CT obtained using Catphan and Gammex phantoms for the three localizations is practically the same for H&N and thorax. However, a difference is observed for pelvis. This can be associated to parameters related to each acquisition protocol. Indeed, the tube voltage has the same value for H&N and thorax, while another value is attributed to pelvis.

Furthermore, HU-ReD curves are dependent on the phantom: For the same ReD, different HU values are obtained with the two phantoms. This effect has been observed for both CT and CBCT imaging modalities. Several authors have already noticed the dependence of calibration curves with the used phantom.[24,25] Indeed, when we compare the calibration curves established with the Catphan phantom compared to those established with the Gammex phantom for the CT acquisitions , a clear difference is visible for densities greater than 1. The curves of the calibration usually have two slopes: the first relates to the low densities of lung and soft tissue and

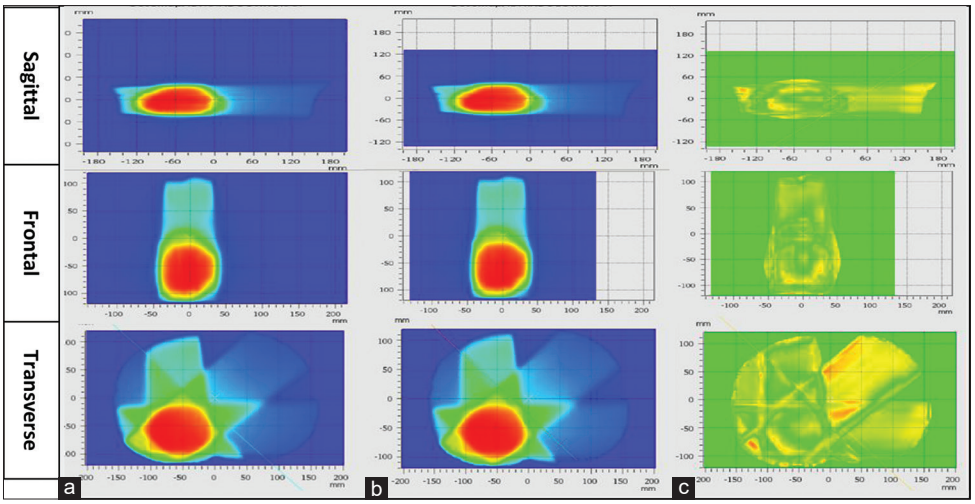

Figure 10: Examples of dose distributions on CT (a), CBCT (b), and results of comparison by gamma index with the criterion 2%, 2 mm (c). CT: Computed tomography, CBCT: Cone beam computed tomography

the second relates to the high densities of bone tissue. Even if the attenuation of photons at the energies considered for the scanner is mainly governed by the Compton effect, the second part of the curve has a larger photoelectric effect fraction than the first part because the probability of the photoelectric effect is proportional to Z^3. The Catphan phantom use a Teflon insert for the determination of the second part of the slope in the calibration curves. However, this material is composed of carbon and fluorite which have a lower atomic number than the calcium and phosphorus of hydroxyapatite constituting bone tissue. Teflon therefore generates less photoelectric effect and leads to lower CT numbers than those found in bone tissue, which explains the low slope of the second part of the curve. Consequently, the dose values which are calculated using these calibration curves will be different.

CBCT image quality is dependent on acquisition parameters and compared with the quality of the planning CT images, exhibit increased artifacts and poorer image contrast owing to increased scatter, which itself is dependent on the size of the scanned object/patient. CBCT images generated using XVI on Elekta treatment units are not in true HU values, and therefore, in their original form, to be able to perform CBCT-based ART, it is important that dose can be calculated accurately (i.e., consistent with that calculated on CT images) on the CBCT image; various methods have been suggested for the adjustment to achieve this, Poludniowski *et al*. have shown that differences, between the doses on CBCT and CT, of less than 2.5% can be achieved when the CBCT has been reconstructed after scatter correction of the individual projections. The implementation of such an approach can be slow and difficult to introduce into a clinical workflow. Commercially available systems that generate CBCTs by using sophisticated scatter-correction algorithms are starting to become commercially available in recent software releases.[12]

As a consequence, the specification of each protocol and its influence on the calibration curves, to obtain a better conversion to relative electronic densities and then a more accuracy in the dose calculation, one should use the adequate calibration curve for each acquisition protocol. According to the relative error of the dose calculation carried out in this study from the CBCT images and relative to the dose calculated from the CT images for the various protocols considered and for the three localizations studied, the error is relatively small when the treatment plan consists of a single beam. This has been observed for all protocols. Then, this error increases with the complexity of the treatment depending on the radiotherapy technique used. However and for a given anatomical location, this error depends on the protocol used. According to these results, one can conclude that the protocols which give better results in terms of dose calculation when compared with dose calculation using CT calibration curves are F0S20 in the H&N region and F1M20 in the thoracic and pelvic regions.

According to the results of the evaluation of these acquisition protocols on the Rando Anderson phantom, for the three locations under study three different pathologies: brain tumor (glioblastoma), lung neoplasia, and prostatic tumor. For each location considered, the dose distributions from CBCT images in the were evaluated for the treatment plans for the protocol chosen was the one that gave the lowest error. These dose calculations were effected using the calibration curves given by the Catphan phantom and those given by the Gammex phantom for the two imaging modalities CT and CBCT.

The percentages of dose differences of target volumes (PTVs) and OARs for H&N, lung neoplasia, and pelvis cases, respectively, performed with the CT images, are less than 1%. This result was predictable since the HU-ReD curves obtained for CT imaging and with the two phantoms were practically identical for the negative ReD values with a slight difference

for the other ReD values compared to the HU-ReD curves obtained with the images CBCT.

Concerning the calculations carried out from the CBCT images, in the case of H&N, the calibration curve obtained with the Gammex phantom gives the best results with errors less than 2% (except for Dmax in optic nerve left (ONL), where the error is less than 3%). For thorax and pelvis, the best results correspond to the calibration curve obtained with the Catphan phantom, where the errors are also less than 1%, except for thorax where there is an error of 3.7% in heart.

This result is well confirmed when we compare the dose distributions obtained from the two imaging modalities using Gamma index. By adopting the 2%, 2 mm criterion for the three planes (sagittal, frontal, and transverse planes) for each location, we find that more than 95% of the points satisfy this criterion.

We can thus deduce that the dose calculation can be performed from the CBCT images with good precision if we use the adequate protocol. Moreover and as already noted by many authors,[26,27] this accuracy can be improved by proceeding to correct the artifacts which exist on the CBCT images.

Conclusion

This study examined the potential feasibility of improving the quality of the dose calculation on CBCT images, by establishing the adequate acquisition parameters and the most appropriate phantom which gives the HU-ReD calibration curves that ensure more precision in the calculation of the CBCT-based dose distribution compared to the CT-based distribution. CBCT images certainly have greater dispersion and artifacts than CT images. Nevertheless, the dosimetric results obtained from the plans applied on CBCT are comparable to those obtained for plans applied on CT with differences that do not exceed 2%, by using the protocols chosen for each anatomy location (F0S20 for H&N and F1M20 for both thorax and pelvis) for the case of use XVI, Elekta. We suggest that, if the CBCT is used for treatment planning purposes, the CBCT should be scanned using the appropriate protocols. Dosimetric data in nonhomogeneous tissue regions must be carefully validated. It is important to note also that better results would be obtained with this method if CBCT images artifacts (such as scattering and beam hardening) are corrected.[26,27]

As a perspective to this study, we will move on to the study on real patients for the different locations to be in the real conditions of an adaptive radiotherapy as a step for the transition to online ART.

Financial support and sponsorship

Nil.

Conflicts of interest

There are no conflicts of interest.

References

1. Jaffray DA, Drake DG, Moreau M, Martinez AA, Wong JW. A radiographic and tomographic imaging system integrated into a medical linear accelerator for localization of bone and soft-tissue targets. Int J Radiat Oncol Biol Phys 1999;45:773-89.
2. Mackie TR, Kapatoes J, Ruchala K, Lu W, Wu C, Olivera G, *et al.* Image guidance for precise conformal radiotherapy. Int J Radiat Oncol Biol Phys 2003;56:89-105.
3. Ghilezan M, Yan D, Martinez A. Adaptive radiation therapy for prostate cancer. Semin Radiat Oncol 2010;20:130-7.
4. Liu H, Wu QA. "Rolling average" multiple adaptive planning methods to compensate for target volume changes in image-guided radiotherapy of prostate cancer. J Appl Clin Med Phys 2012;13:124-37.
5. Yoo S, Yin FF. Dosimetric feasibility of cone-beam CT-based treatment planning compared to CT-based treatment planning. Int J Radiat Oncol Biol Phys 2006;66:1553-61.
6. Reggiori G, Mancosu P, Tozzi A, Cantone MC, Castiglioni S, Lattuada P, *et al.* Cone beam CT pre- and post-daily treatment for assessing geometrical and dosimetric intrafraction variability during radiotherapy of prostate cancer. J Appl Clin Med Phys 2010;12:3371.
7. Yohannes I, Prasetio H, Kallis K, Bert C. Dosimetric accuracy of the cone-beam CT-based treatment planning of the Vero system: A phantom study. J Appl Clin Med Phys 2016;17:106-13.
8. Barateau A, Garlopeau C, Cugny A, De Figueiredo BH, Dupin C, Caron J, *et al.* Dose calculation accuracy of different image value to density tables for cone-beam CT planning in head & neck and pelvic localizations. Phys Med 2015;31:146-51.
9. Barateau A, Céleste M, Lafond C, Henry O, Couespel S, Simon A, *et al.* External beam radiotherapy cone beam-computed tomography-based dose calculation. Cancer Radiother 2018;22:85-100.
10. Yang Y, Schreibmann E, Li T, Wang C, Xing L. Evaluation of on-board kV cone beam CT (CBCT)-based dose calculation. Phys Med Biol 2007;52:685-705.
11. Ali ES, Webb R, Nyiri BJ. Rotational artifacts in on-board cone beam computed tomography. Phys Med Biol 2015;60:1461-76.
12. Dunlop A, McQuaid D, Nill S, Murray J, Poludniowski G, Hansen VN, *et al*. Comparison of CT number calibration techniques for CBCT-based dose calculation. Strahlenther Onkol 2015;191:970-8.
13. Lu W, Olivera GH, Chen Q, Ruchala KJ, Haimerl J, Meeks SL, *et al.* Deformable registration of the planning image (kVCT) and the daily images (MVCT) for adaptive radiation therapy. Phys Med Biol 2006;51:4357-74.
14. Hu W, Ye J, Wang J, Ma X, Zhang Z. Use of kilovoltage X-ray volume imaging in patient dose calculation for head-and-neck and partial brain radiation therapy. Radiat Oncol 2010;5:29.
15. Richter A, Hu Q, Steglich D, Baier K, Wilbert J, Guckenberger M, *et al.* Investigation of the usability of conebeam CT data sets for dose calculation. Radiat Oncol 2008;3:42.
16. de Smet M, Schuring D, Nijsten S, Verhaegen F. Accuracy of dose calculations on kV cone beam CT images of lung cancer patients. Med Phys 2016;43:5934.
17. Posiewnik M, Piotrowski T. A review of cone-beam CT applications for adaptive radiotherapy prostate cancer. Phys Med 2019;59:13-21.
18. Giacometti V, Hounsell AH, McGarry CK. A review of dose calculation approaches with cone beam CT in photon and proton therapy. Phys Med 2020;76:243-76.
19. Barateau A, De Crevoisier R, Largent A, Mylona E, Perichon N, Castelli J, *et al.* Comparison of CBCT-based dose calculation methods in head and neck cancer radiotherapy: From Hounsfield unit to density calibration curve to deep learning. Med Phys 2020;47:4683-93.
20. Mail TB, Catphan 500 and 600 Manual, The Phantom Laboratory,Inc. Greenwich, NY, USA 2006. p 17.
21. Constantinou C, Harrington JC, DeWerd LA. An electron density calibration phantom for ct-based treatment planning computers. Med

Phys. 1992;19:325-7.
22. Atlas Anatomy: Michael Pretterklieber. In:MR/CT Atlas of Anatomy (CD-ROM), Edited by Klaus Kueper, Thieme, 2001. ISBN 3-13-129991-6.
23. Available from: https://www.ptwdosimetry.com/en/products/verisoft/. [Last accessed on 2020 Dec 20].
24. Hatton J, McCurdy B, Greer PB. Cone beam computerized tomography: The effect of calibration of the Hounsfield unit number to electron density on dose calculation accuracy for adaptive radiation therapy. Phys Med Biol 2009;54:N329-46.
25. Guan H, Dong H. Dose calculation accuracy using cone-beam CT (CBCT) for pelvic adaptive radiotherapy. Phys Med Biol 2009;54:6239-50.
26. Schulze R, Heil U, Gross D, Bruellmann DD, Dranischnikow E, Schwanecke U, *et al.* Artefacts in CBCT: A review. Dentomaxillofac Radiol 2011;40:265-73.
27. Park YK, Sharp GC, Phillips J, Winey BA. Proton dose calculation on scatter-corrected CBCT image: Feasibility study for adaptive proton therapy. Med Phys 2015;42:4449-59.